Physics of Plasmas ARTICLE scitation.org/journal/php

The effects of multipactor on the quality of a complex signal propagating in a transmission line

Cite as: Phys. Plasmas **26**, 112114 (2019); doi: 10.1063/1.5125408
Submitted: 22 August 2019 · Accepted: 28 October 2019 ·
Published Online: 15 November 2019

Patrick Y. Wong,[1,2] Y. Y. Lau,[1,a)] Peng Zhang,[2] Nicholas Jordan,[1] Ronald M. Gilgenbach,[1] and John Verboncoeur[2]

AFFILIATIONS

[1]Department of Nuclear Engineering and Radiological Sciences, University of Michigan, Ann Arbor, Michigan 48109, USA
[2]Department of Electrical and Computer Engineering, Michigan State University, East Lansing, Michigan 48824, USA

[a)]Author to whom correspondence should be addressed: yylau@umich.edu

ABSTRACT

Multipactor is a much studied resonant AC discharge that is harmful to microwave components and circuits. There is substantial current interest in this topic because of its threat to satellite communications. In this paper, an analytical transmission line model is presented to assess the effects of multipactor, should it happen, on the distortion of a signal. The model is applicable to any input signal (analog or digital) once the electron multipactor current it causes is specified. Examples using planar and coaxial transmission lines are given on a simple dynamical model of the multipactor current. Single and multitone signals are treated, with some results presented in the In-phase and Quadrature plots.

I. INTRODUCTION

Multipactor is a radio frequency (RF) discharge, which threatens telecommunications systems, high power microwave sources, and accelerator structures. Under certain conditions, multipactor may dissipate power, degrade performance, increase system noise, and in the worst scenario, lead to the complete destruction of the microwave components.[1,2]

In recent years, the restricted frequency spectrum and the cluttered satellite orbits require a single spacecraft to perform the same or enhanced functions, which previously required several satellites.[3] This necessitates complex multifrequency operation for a much enlarged orbital capacity and mission. High power RF payload is required, which significantly increases the threat of multipactor. The degradation of signal quality has become a major concern.[3,4] Signal distortion and unwanted frequencies may be generated actively, for example, by multipactor,[5–12] or passively,[13] by the nonlinear electrothermal effect,[14] dirty contacts,[15] or ferroelectric materials inherent to the microwave components.[16] This paper proposes a method to quantify the effects of multipactor on the quality of the signal that propagates along a transmission line (TL). We note that this work is different from previous studies[17–21] where the main focus there was establishing the "threshold" for multipactor; here, we assume that multipactor is already initiated by some process and observe how this will affect the signal to be transmitted. The algorithm is applicable to any complex signal once the multipactor current is specified. We illustrate the use of this procedure with examples, using both a parallel plate transmission line (e.g., Refs. 1, 2, 8, 11, 19, and 22) and a coaxial transmission line (e.g., Refs. 9, 10, 17, 18, 20, 21, and 23–27).

Given the right conditions (RF fields, geometry, etc.), a stray electron born from various processes (e.g., cosmic rays) may initiate multipactor discharge. Since we are mainly interested in the effects of multipactor on the signal quality, we assume that the multipactor has not reached the level to cause significant loading of the RF structure. That is, the multipactor, generated by the complex signal, causes a small perturbation on the wall current of the RF structure, which then contaminates the signal quality at the output.[28] We quantify this process using a transmission line model. The evolution of the multipactor current is highly complex. It is model dependent and is treated separately, an example of which is given in Sec. III. Once the multipactor current is specified, either from analytical modeling or simulation results, our algorithm immediately yields its effect on signal quality, for a general complex signal.

In Sec. II, we explicitly calculate the effects on the complex signal due to a time-dependent multipactor current that is generated at some position along the transmission line through which the signal propagates. In Sec. III, we concentrate on the highly idealized, but nontrivial model of multipactor current on a coaxial transmission line, where single surface and two-surface multipactor can simultaneously occur.[29–31] In Sec. IV, we present numerical examples, in which the signal may contain multiple frequencies, with some results displayed

in the In-phase and Quadrature (I-Q) plots. Section V gives concluding remarks.

II. THE TRANSMISSION LINE MODEL

The transmission line model is shown in Fig. 1. The transmission line is assumed to be lossless and has characteristic impedance Z_0. Mismatches are allowed at the source (at $z=0$) and load (at $z=l$) through their termination impedances, Z_S and Z_L, respectively. The complex signal is modeled by the voltage source $V_S(t)$ located at $z=0^-$. Multipactor is modeled as a local current source, $I_m(t)$, that is placed at $z=z_m$ along the transmission line. Once $V_S(t)$ and $I_m(t)$ are specified, the voltage $V(z,\ t)$ on the transmission line may be calculated explicitly. We write

$$V(z,t) = V_1(z,t) + V_2(z,t), \tag{1}$$

where $V_1(z,\ t)$ is the voltage due only to the input signal V_S (i.e., no multipactor) and $V_2(z,t)$ is the voltage perturbation due to multipactor current, I_m. We show in Appendix A that, for all values of z between 0 and l,

$$V_1(z,t) = \frac{Z_0}{Z_0+Z_S}\sum_{n=0}^{\infty}\left\{(R_LR_S)^n V_s\left(t-\left(\frac{2nl}{v}+\frac{z}{v}\right)\right)\right.$$
$$\left.+R_L(R_LR_S)^n V_s\left(t-\left(\frac{2(n+1)l}{v}-\frac{z}{v}\right)\right)\right\}, \tag{2}$$

$$V_2(z,t) = V_2^{(+)}(z,t) + V_2^{(-)}(z,t), \tag{3}$$

$$V_2^{(+)}(z,t) = \frac{Z_0}{2}\sum_{n=0}^{\infty}\left\{(R_LR_S)^n\left[I_m\left(t+\frac{z_m}{v}-\left(\frac{2nl}{v}+\frac{z}{v}\right)\right)\right.\right.$$
$$\left.\left.+R_LI_m\left(t+\frac{z_m}{v}-\frac{2(n+1)l}{v}+\frac{z}{v}\right)\right]\right\}, \tag{4a}$$

$$V_2^{(-)}(z,t) = \frac{Z_0}{2}\sum_{n=0}^{\infty}\left\{(R_LR_S)^n\left[I_m\left(t-\frac{z_m}{v}+\left(\frac{2nl}{v}+\frac{z}{v}\right)\right)\right.\right.$$
$$\left.\left.+R_SI_m\left(t-\frac{z_m}{v}+\frac{2(n+1)l}{v}-\frac{z}{v}\right)\right]\right\}, \tag{4b}$$

$$\begin{cases} R_S = \dfrac{Z_S-Z_0}{Z_S+Z_0} \\ R_L = \dfrac{Z_L-Z_0}{Z_L+Z_0}. \end{cases} \tag{5}$$

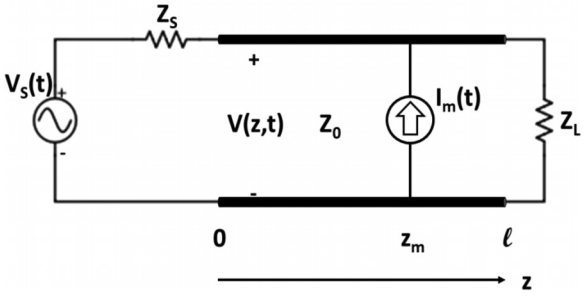

FIG. 1. Transmission line model to analyze the effects of multipactor on the quality of a signal.

In these equations, R_S and R_L are the reflection coefficients at the source and load, respectively, v is the phase speed of the traveling wave on the line, taken here to be the speed of light in vacuum, $V_2^{(+)}$ is the contribution from the portion of the multipactor current that originally propagates to the right of z_m, and $V_2^{(-)}$ is the contribution from the portion of the multipactor current that originally propagates to the left of z_m. Regardless of the complexity in $V_S(t)$ and $I_m(t)$, the contamination of the signal by multipactor at the load is given explicitly by $V_2(l,t)$ in Eq. (3). Note that if there is a spatial distribution of multipactor current along the transmission line, a simple superposition of Eq. (3) would yield the signal degradation from such a spatial distribution of multipactor current. Thus, in Sec. III, we give an explicit calculation, for a coaxial transmission line model, of the multipactor current, $I_m(t)$ that is restricted to the axial position z_m.

III. A MULTIPACTOR MODEL

In this section, we shall concentrate on the formulation of multipactor in a coaxial transmission line. The much simpler case of a planar transmission line will be commented on toward the end of this section. The temporal evolution of the multipactor current caused by an electron that is initially located in a coaxial transmission line at $z=z_m$ is a very complex problem. An accurate description requires these considerations: the initial velocity of the electron, initial phase of the RF electric field of the complex signal that it experiences, the subsequent electron trajectory, the type of multipactor (both the single surface and two-surface can simultaneously occur in a coaxial transmission line), the order of the multipactor, the impacting energy and impact angle for the generation of secondary electrons, the model for secondary electron yield, and the distribution of the secondary electron emission velocity. The induced wall current, modeled by $I_m(t)$ in Fig. 1 and due to the motion of the multipacting electrons, is then obtained from the Ramo-Shockley Theorem.[32] Inclusion of all of these complex features would require a 3-dimensional particle-in-cell code.

To make some progress in the understanding, we use an analytical formulation and make the following assumptions: (a) all secondary electrons are emitted from a surface with monoenergetic initial velocity; (b) all electron motions are purely radial; (c) the electrons are modeled as an infinitesimally thin cylindrical shell, located in the immediate vicinity of $z=z_m$, where it executes radial motion; (d) the acceleration on this cylindrical shell is calculated by assuming that it has a long axial length, subject to the instantaneous voltage $V_1(z_m,t)$ due to the complex signal [cf. Eq. (2)]. The additional force due to the image charges of the cylindrical shell may then be much more readily accounted for; (e) upon impact on a surface, the incident electron shell is removed, and a new one is released whose charge density (and mass density) is multiplied by δ, the secondary yield coefficient according to a modified Vaughan model,[33,34] and there is no time delay in the emission of secondary electrons; (f) the wall current, $I_m(t)$, is calculated by the Ramo-Shockley Theorem[32] when the electron shell is in transit.

There are deficiencies on each of the assumptions. Here, we only note that the use of the electron sheet model to calculate $I_m(t)$, in particular in the image charge forces and in the application of the Ramo-Shockley Theorem, has been used in previous studies of two-surface multipactor.[2,11,23,24] Similar electron sheets have also been adopted in the study of single surface multipactor on a dielectric surface.[12,35–37] Our 1D model here (for illustrative purposes) restricts us to a slice of parameter space. A more accurate description of reality would

necessitate the use of a full 3-dimensional particle-in-cell code, where we expect the multipactor threshold to be shifted because of the added degrees of freedom in motion for secondary electron yield (e.g., electrons are no longer impacting the surface at normal incidence and hence at full energy). The use of $V_1(z_m, t)$ in assumption (d), in the form of Eq. (2), means that the multipactor current is assumed to be at a sufficiently low level; it has not caused any significant change in the input signal throughout.

A similar electron sheet model for multipactor in a coaxial geometry was adopted by Udiljak *et al.*[23] and by Sorolla *et al.*[24] We shall use it here, with some similar parameters. The force law for this electron sheet reads (for the coaxial geometry)

$$m_e \frac{d^2\rho'}{dt^2} = \frac{1}{\rho'}\left[\Lambda_1 \ln\left(\frac{\rho'^2}{ab}\right) - \Lambda_2 V(t)\right], \tag{6}$$

where $\Lambda_1 = \frac{e^2 N_e(t)}{4\pi\epsilon_0 l \ln\left(\frac{b}{a}\right)}$ and $\Lambda_2 = \frac{e}{\ln\left(\frac{b}{a}\right)}$, ρ' is the radial location of an electron (mass m_e, charge-e) in the electron sheet, a and b are the radii of the inner and outer coaxial line, respectively, $V(t) = V_1(z_m, t)$ is the time-varying voltage waveform at the location of multipaction, due only to the input signal [cf. Eq. (2)], and $N_e = N_e(t)$ is the number of electrons in the electron sheet, which changes when the sheet (of primary electrons) impacts the inner or outer conductor and secondary electrons are released. In the RHS of Eq. (6), the first term is the image charge term due to the electron sheet (This term is referred to as the "space-charge" term in the literature, but it is more accurately called the "image charge" term because it does not take into account mutual space-charge repulsion.), and the second term is due to the time-varying electric field of the signal. The multipactor current, $I_m(t)$ in Fig. 1, may then be determined using the Ramo-Shockley Theorem (for coaxial geometry)[32] as

$$I_m(t) = \frac{eN_e(t)}{\log\left(\frac{b}{a}\right)} \frac{1}{\rho'(t)} \frac{d\rho'}{dt}. \tag{7}$$

Equation (3) then explicitly gives the contamination of the input signal by multipactor due to the multipactor current, $I_m(t)$.

For a planar transmission line, the orbital equation (6), and the expression for the multipactor current, (7), may be easily obtained by letting both a and b tend to infinity, with $D = b - a$ approaching a finite value (D is the spacing between the parallel plate transmission lines).

IV. NUMERICAL EXAMPLES

We consider several examples here as a demonstration of the model. In these examples, we assume that the secondary electron emission coefficient, δ, is governed by a modified Vaughan model,[33,34] corrected to better capture the low energy impacts below the threshold energy (where reflections of the primary electrons from the surface become exceedingly important). The threshold energy $E_{threshold}$ itself is also allowed to vary to fit the experimentally determined first crossover energy E_1 for the material of the electrodes. The emission of secondary electrons from the surface is monoenergetic (E_0). The maximum secondary electron yield is δ_{max}, occurring at impact energy E_{max} of a primary electron.

First, we will look at a simple planar case. We will then look at single-surface and two-surface coaxial multipactor. In the two-surface case, we will consider both a single-tone signal and then a dual-tone signal with different frequency separations between the two tones. In all of the examples, the source voltage has the form: $V_S(t) = V_{S,\max}\left[\sin(\omega_1 t) + \beta\sin(\omega_2 t + \gamma)\right]$, initiating a voltage on the line at $z = 0^+$ with the form $V(t) = V_{RF}\left[\sin(\omega_1 t + \alpha) + \beta\sin(\omega_2 t + \alpha + \gamma)\right]$, with two frequencies ω_1 (first tone) and ω_2 (second tone). Here, β and γ are the relative amplitude and phase of the second tone to the first and α is the launch phase of the electron with respect to the voltage signal of the first tone (to account for the phase of the multipacting electrons). From Fig. 1, we find $V_{RF} = \frac{Z_0}{Z_0 + Z_S} V_{S,\max}$. The effect of the multipactor current will be monitored at the output, $z = l$.

The parameters for the planar case are tabulated in Table I. The main results are shown in Fig. 2. Figure 2(a) shows the transmitted signal without any errors. Figure 2(b) shows the error in the signal voltage at the load due to localized multipactor at $z = z_m$. Note that the multipactor current saturates; this saturation is due to space-charge.[22,24] Figure 2(b) shows that $\max(V_2) \sim 2$ V, so multipactor introduces an ~0.6% error to the signal, amplitude-wise. This voltage waveform due only to multipactor may be decomposed into an "I (In-phase)" component (which is in phase with the original signal) and the orthogonal "Q (Quadrature)" component (see Appendix B). A parametric plot showing the temporal evolution of these two components is given in Fig. 2(c). Figure 2(c) containing this "I-Q" plot is another graphical representation of the error introduced by multipactor: at any point on the plot, the amplitude of the error is $\sqrt{I^2 + Q^2}$ relative to the pristine case (the origin) and the phase of the error is the angle measured from the I-axis. To help in relating the error in the voltage signal due to multipactor [Fig. 2(b)] to its I-Q representation [Fig. 2(c)], two time markers that mark important events have been placed in both figures. It should be noted that the I-Q diagram in Fig. 2(c) exaggerates the period up until multipactor saturates. "I" oscillates with time, while "Q" increases with time until multipactor saturation. At saturation, Q is near constant while I continues to oscillate in time with a reduced period.

We next consider the coaxial transmission line, a more complicated case. The parameters for single-surface multipactor are tabulated in Table II; the results are shown in Fig. 3. Two-surface multipactor may also occur in a coaxial setup; a test case for such a phenomenon is shown in Table III with the corresponding results in Fig. 4. Finally, coaxial systems with dual-tone signals are also studied. The setup looked at here is based on the two-surface setup in Table III with some

TABLE I. Tabulation of parameters for a test case with a planar transmission line.

Planar transmission line parameters					
Circuit		Dimensions		Material	
$V_{S,max}$	350 V	D	0.22 cm	δ_{max}	1.2
f	1 GHz	A	0.25 cm^2	E_{max}	400 eV
z_m	0.3 m				
l	0.5 m	Multipactor electrons			
$Z_0 = Z_S = Z_L$	50 Ω	$N_e(t=0)$	1.4×10^6		
		E_0	0 eV		

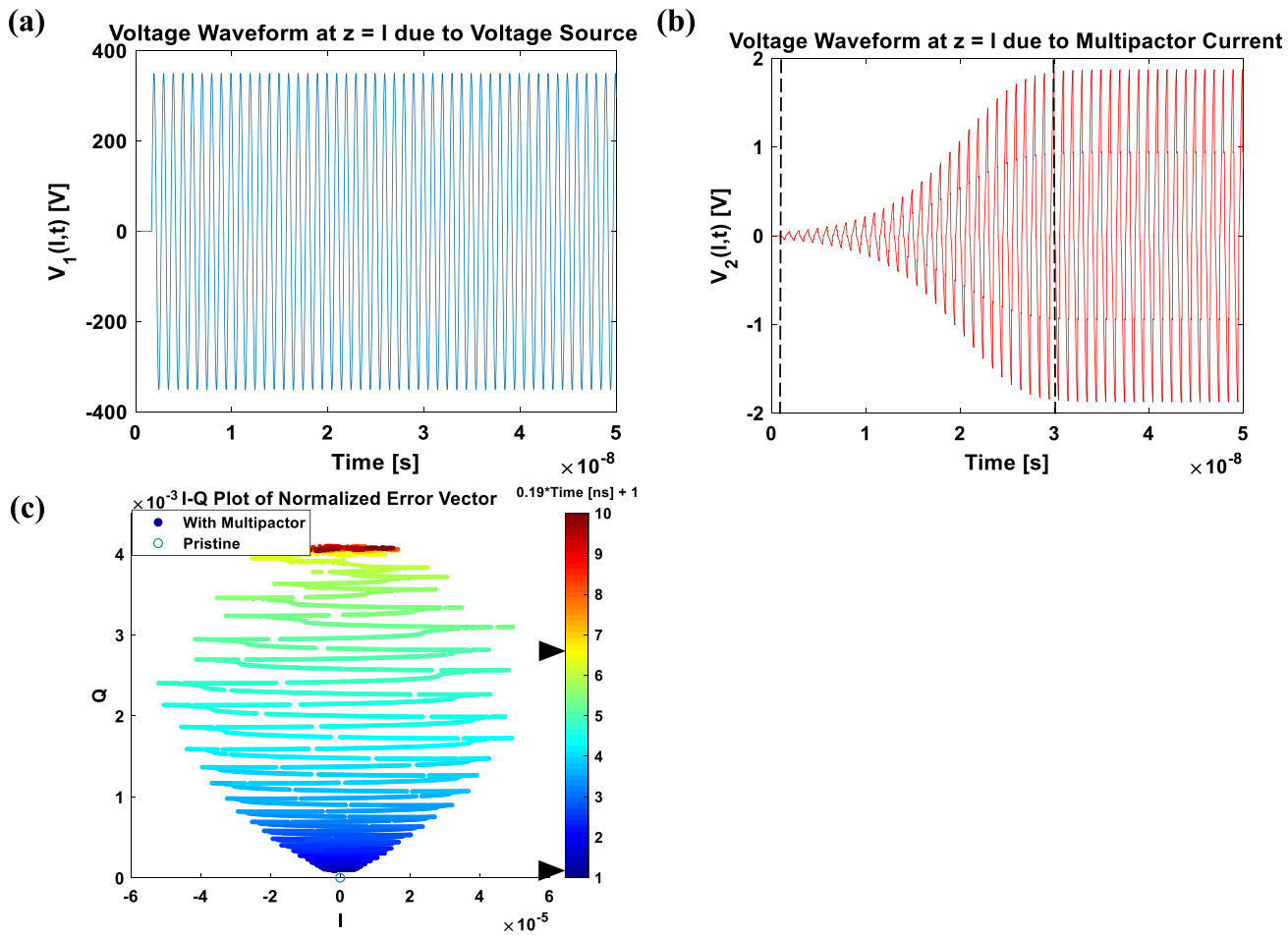

FIG. 2. Transmission line voltage at the output $z = l$ as a function of time for the planar transmission line (cf. Table I). (a) The signal voltage without multipactor (blue) and (b) the voltage perturbation due to multipactor (red). (c) I-Q plot of the normalized error due to multipactor. Two time markers (black) are shown in (b) and (c).

minor adjustments presented in Table IV. The main results for the two-tone signal study are shown in Figs. 5 and 6.

Similar to Fig. 2, Fig. 3 shows the voltage waveforms that result from a sinusoidal input into the transmission line without multipactor (blue) and the resulting perturbation due to the signal-induced localized multipactor (red). The characteristic waveform due to multipactor is a direct result of the single-surface multipactor exhibited by this system [the trajectories of these electrons are also shown in Fig. 3(c)]. In Fig. 3(d), there is a jump from the pristine case at $t = 0$. The reason is because we are inspecting the perturbation from multipactor at the output ($z = l$), but multipactor has already started distorting the signal in the finite propagation time between its initiation at $z = z_m$ and its arrival at the output. Amplitude-wise, multipactor here introduces a maximum of ∼3% error to the signal, but it is also evident that there is phase modulation in addition to amplitude modulation (as is the case with all of the examples shown here).

Figure 4 shows the growth of the electron population and the corresponding current in the system of two-surface coaxial multipactor over the time span of 2 μs. The growth, transition to saturation, and saturation may be seen in these plots. A scatterplot of the electron impact energy with the outer and inner electrodes is also shown; $\delta_{avg} > 1$ due to the asymmetry of the coaxial system, favoring the outer electrode in terms of impact energy. The three distinct regions of multipactor growth, transition to saturation, and saturation may also

TABLE II. Tabulation of parameters for a test case with single-surface multipactor in a coaxial transmission line.

Coaxial transmission line parameters: single-surface multipactor					
Circuit		Dimensions		Material: silver	
$V_{S,max}$	2400 V	a	5 mm	δ_{max}	2.22
f	3 GHz	b	10 mm	E_{max}	165 eV
z_m	0.1 m			E_1	30 eV
l	1 m	Multipactor electrons		k_θ, k_E	1, 1
$Z_0 = Z_S = Z_L$	41.56 Ω	$N_e(t = 0)$	10^6	$E_{threshold}$	17 eV
		E_0	0 eV		

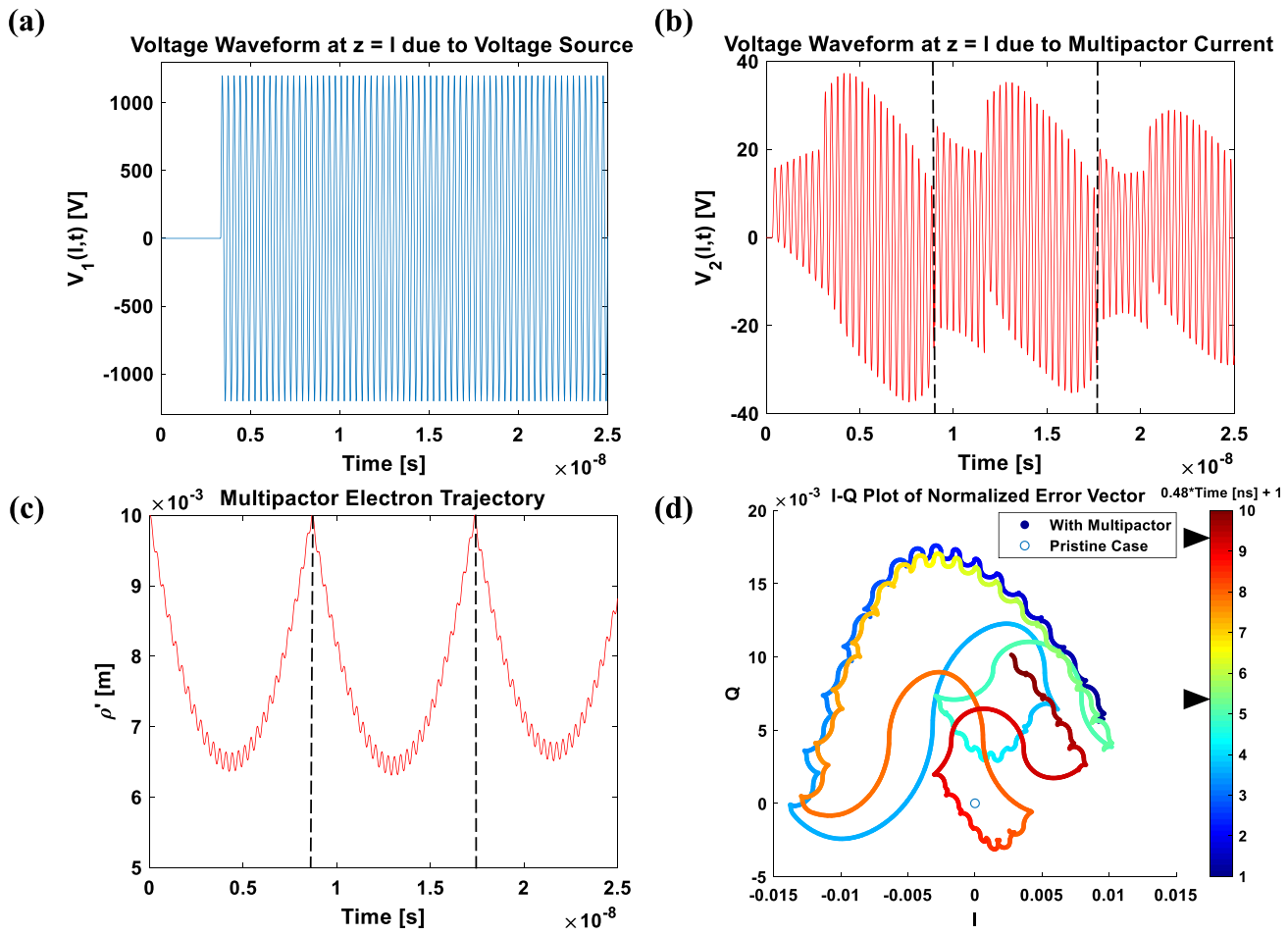

FIG. 3. Single-surface coaxial multipactor test case results (cf. Table II): (a) the voltage waveform of the signal without multipactor (blue) at the output; (b) the voltage waveform of the perturbation due to multipactor (red) at the output; (c) a plot of the multipactor electron sheet trajectory at the location of multipaction. Note how the electrons never reach the inner electrode; (d) I-Q plot of the normalized error due to multipactor. Two time markers (black) are shown in (b), (c), and (d).

be seen in the plot of the time evolution of the error due to multipactor in the voltage signal waveform. It is interesting to note that the voltage waveform here is similar to the planar case in Fig. 2 (which also exhibited two-surface multipactor) with the exception of the asymmetry in amplitude due to the asymmetry in radial particle motion in this coaxial system. A rough estimate (inspecting amplitude) gives an ∼5% error to the signal due to multipactor.

TABLE III. Tabulation of parameters for a test case with two-surface multipactor in a coaxial transmission line.

Coaxial transmission line parameters: two-surface multipactor					
Circuit		Dimensions		Material: silver	
$V_{S,max}$	120 V	a	1 mm	δ_{max}	2.22
f	1 GHz	b	2 mm	E_{max}	165 eV
z_m	0.3 m			E_1	30 eV
l	1 m	Multipactor electrons		k_θ, k_E	1, 1
$Z_0 = Z_S = Z_L$	41.56 Ω	$N_e(t=0)$	1	$E_{threshold}$	17 eV
		E_0	0.3 eV		

Figures 5 and 6 capture the main results of the coaxial case with a dual-tone signal as an input. When the frequency separation between the two tones is 1 MHz, multipactor is suppressed[38] after a relatively brief amount of time, as evidenced by Fig. 5. There is a very insignificant burst of multipactor error early in time before decaying to zero. However, when the frequency separation between the two tones is increased to 10 MHz, multipactor grows as can be seen in Fig. 6. A look at the scatterplot of impact energy on the electrodes as a function of time suggests a periodic pattern, matching the beat wave generated by the two tones. In terms of the error introduced by multipactor, the voltage perturbation is sporadic, coming in bursts but never decaying to zero. The multipactor electrons in the sheet also exhibit a combination of single-surface and two-surface trajectories. For the I-Q plots, the error introduced to each tone individually is given in Figs. 5(d) and 6(f) (cf. last paragraph of Appendix B).

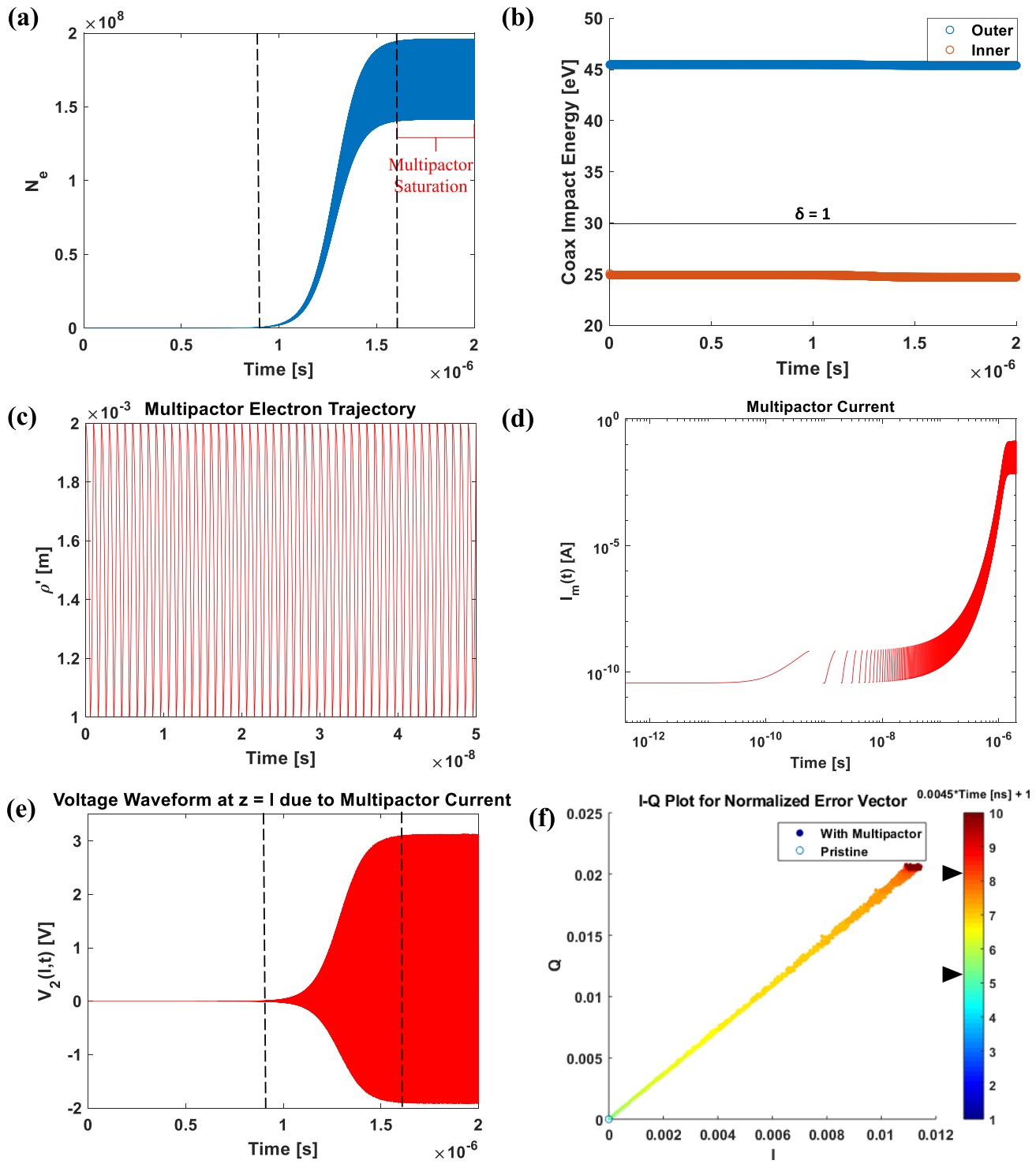

FIG. 4. Two-surface coaxial multipactor test case results (cf. Table III): (a) the growth of the multipactor electron population, including multipactor saturation, is shown; (b) a plot of the impact energy on both the outer and inner electrodes as a function of time is shown; (c) the plot shows a sample of the electron sheet trajectory, demonstrating explicit two-surface multipactor; (d) a log-log plot of the multipactor current as a function of time also shows the growth and saturation of multipactor; (e) the time evolution of the error in voltage is given. Note the asymmetry in the amplitude; (f) I-Q plot of the normalized error due to multipactor. Two time markers (black) are shown in (a), (e), and (f).

TABLE IV. Tabulation of parameters for a test case with a dual-tone signal in a coaxial transmission line.

Coaxial transmission line parameters: dual-tone multipactor ($\beta = 1, \gamma = 0$)					
Circuit		Dimensions		Material: silver	
f	1 GHz	a	1 mm	δ_{max}	2.22
z_m	0.3 m	b	2 mm	E_{max}	165 eV
l	1 m			E_1	30 eV
$Z_0 = Z_S = Z_L$	41.56 Ω	Multipactor electrons		k_θ, k_E	1, 1
		$N_e(t = 0)$	1	$E_{threshold}$	17 eV
		E_0	0.3 eV		
		$\Delta f = 1$ MHz			
	$V_{S,max}$			63 V	
		$\Delta f = 10$ MHz			
	$V_{S,max}$			66.25 V	

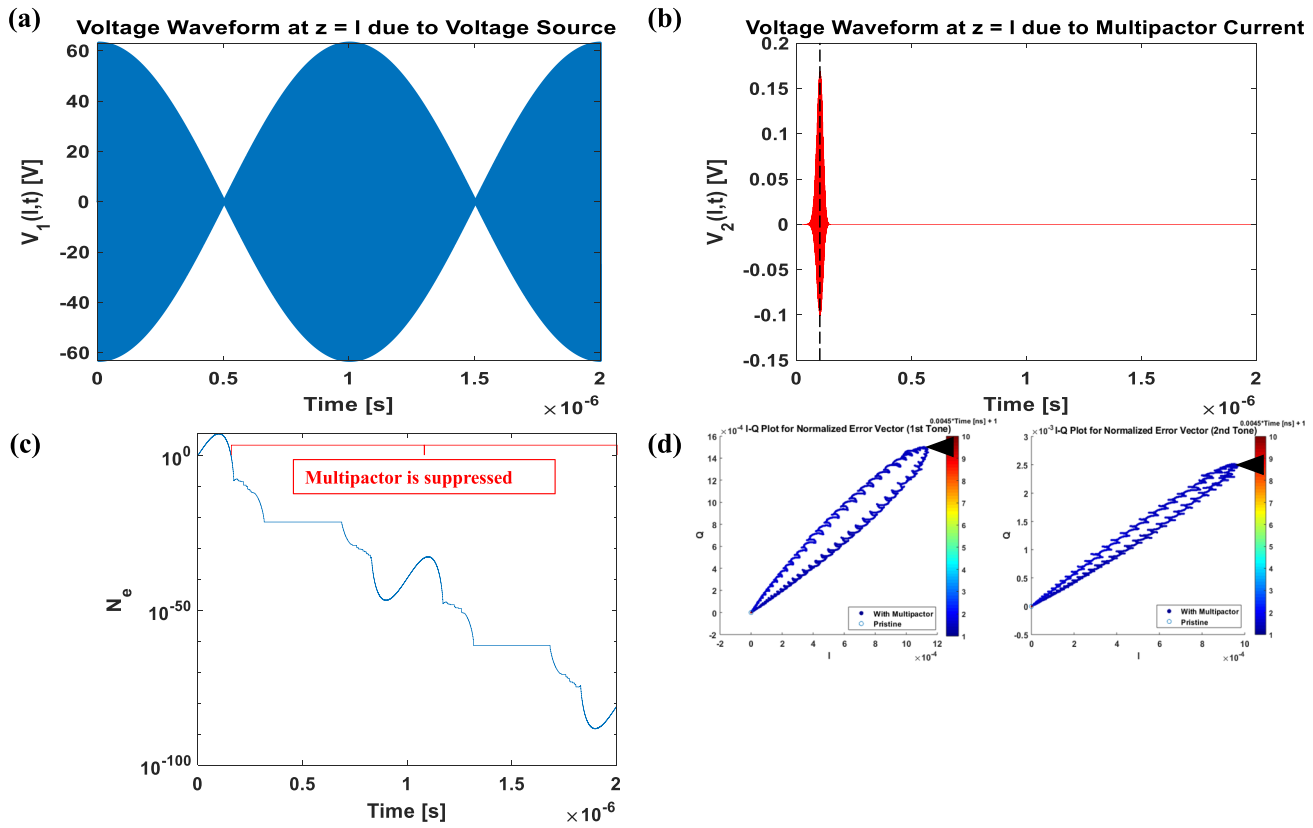

FIG. 5. Two-surface coaxial multipactor with two-tone signals of 1 MHz separation test case results (cf. Tables III and IV): the time evolutions of the (a) original signal (blue) and the (b) error in voltage (red) are given; (c) the decay of the multipactor electron population is shown; (d) I-Q plots of the normalized error due to multipactor. A time marker (black) is shown in (b) and (d).

V. CONCLUDING REMARKS

In this paper, the effects of signal-induced localized multipactor on a signal that propagates along a transmission line have been analyzed. A closed form, time-domain solution is obtained in terms of the localized multipactor current. It was first applied to a single-tone, two-surface multipactor in a planar transmission line. For the more complicated coaxial geometry, single-tone, single-surface, and two-

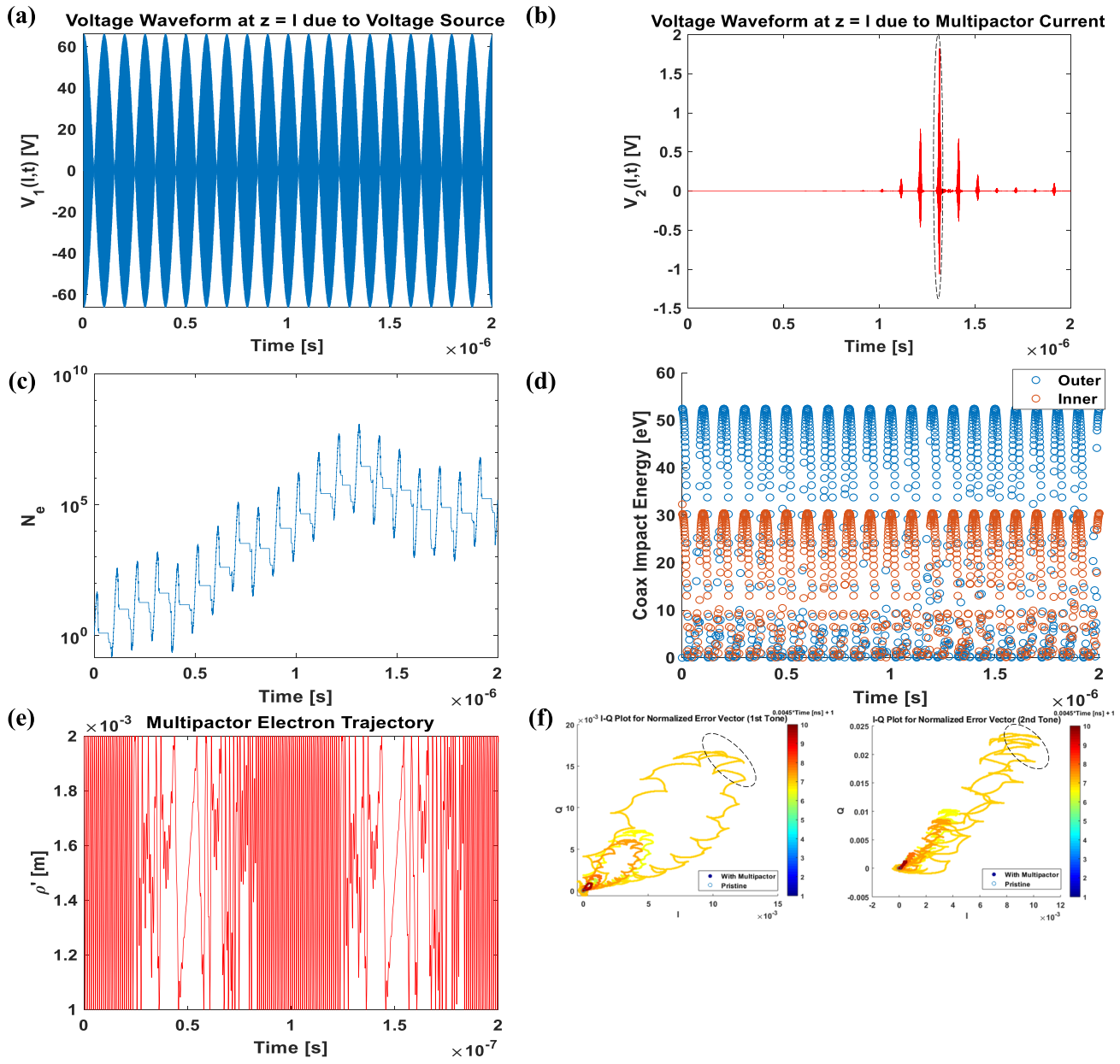

FIG. 6. Coaxial multipactor with two-tone signals of 10 MHz separation test case results (cf. Tables III and IV): the time evolutions of the (a) original signal (blue) and the (b) error in voltage (red) are given. Note the sporadic nature of multipactor in (b); (c) the growth of the multipactor electron population is shown; (d) a plot of the impact energy on both the outer and inner electrodes as a function of time is shown; (e) a sample plot of the electron trajectory is also given, showing a mix of single-surface and two-surface multipactor; (f) I-Q plots of the normalized error due to multipactor. A time marker (black) is shown in (b) and (f).

surface multipactor cases were investigated, followed by an extension to a two-tone case. In all cases regardless of geometry and signal drive, it was found that the error on the signal due to multipactor has a magnitude roughly proportional to the multipactor current induced by the original signal. Both the amplitude and phase modulation were apparent in the distorted signal after multipactor was introduced. In the parameter space investigated here, the perturbation amplitude due to multipactor was at most a single-digit percentage of the original transmission line signal. Nevertheless, in the course of this study, it was found that there is a subtle boundary between appreciable and overwhelming multipactor. For example, in the two-tone cases keeping all parameters constant and changing only the RF voltage amplitude (not shown), there was a very sharp boundary between multipactor as seen in Figs. 5 and 6 and overwhelming multipactor that completely

destroyed the signal (>100% of voltage signal amplitude). The most severe case seen was in Fig. 6, where a ∼1% change to $V_{S,max}$ led to overwhelming multipactor. We also found that in the two-tone case, multipactor can be suppressed or be made sporadic depending on the frequency separation of the tones.

Since the major emphasis of this paper is in the effects of multipactor on the signal quality, we assume that the multipactor does not significantly distort the signal (i.e., loading is unimportant). Nor do we consider the startup condition in any detail. We simply assumed that a seed electron exists somewhere on the transmission line and it is subjected to an instantaneous complex signal. The calculation of the multipactor current is an enormously complicated task. The electron trajectory, and its subsequent generation of secondary electrons, is highly model dependent. The results depend not only on the complex signal, they are also highly dependent on the secondary electron yield model, the assumed secondary electrons' initial velocity distribution, the transmission line geometry, and the mutual interaction among the multipacting electrons. Thus, the generation of the multipactor current $I_m(z, t)$ needs to be done separately, e.g., from a separate numerical code, or a numerical code branded with analytical models. Once $I_m(z, t)$ is obtained, its effect on signal quality may be immediately applied using Eq. (3) or its straightforward extensions. In this sense, our model is rather general. While this paper only considers analog signals, it would be of interest to apply to digitally modulated (discrete) signals, and to investigate how multipactor, should it occur, may affect the I-Q (In-phase, Quadrature) components (constellation diagrams) of a digital signal. Future work may also include allowing for impedance mismatches in the source and load to analyze the effects of reflections on multipactor stability and carrier cross coupling.

ACKNOWLEDGMENTS

We thank David Chernin for useful discussions. This work was supported by AFOSR MURI Grant No. FA9550-18-1-0062, AFOSR Grant No. FA9550-15-1-9007, and by the L3 Technologies Electron Devices Division.

APPENDIX A: DERIVATION OF THE TRANSMISSION LINE MODEL

In this Appendix, the combined effects on a complex signal by a multipactor current and by the end reflections of a transmission line (TL) into which the complex signal is launched will be studied. Equations (1)–(4) of the main text will be derived. The setup is the same as in Fig. 1 of the main text.

We assume that the complex waveforms of the voltage source, $V_S(t)$, and the multipactor current, $I_m(t)$, are specified. They become ideal voltage and current sources in Fig. 1. The voltage $V(z, t)$ on the TL may then be obtained explicitly, in closed form, by superposition. Since $V_S(t)$ and $I_m(t)$ are assumed to be ideal voltage and current sources, we may decompose the voltage $V(z, t)$ on the TL in the manner shown in Eq. (1), where $V_1(z, t)$ is the voltage on the TL due to the voltage source $V_S(t)$ alone, setting $I_m(t) = 0$, as shown in Fig. 7(a), and $V_2(z, t)$ is the voltage on the TL due to the current source $I_m(t)$ alone, setting $V_S(t) = 0$, as shown in Fig. 7(b). We will show below that $V_1(z, t)$ is given by Eq. (2) and that $V_2(z, t)$ is given by Eq. (3), for arbitrary $V_S(t)$ and $I_m(t)$.

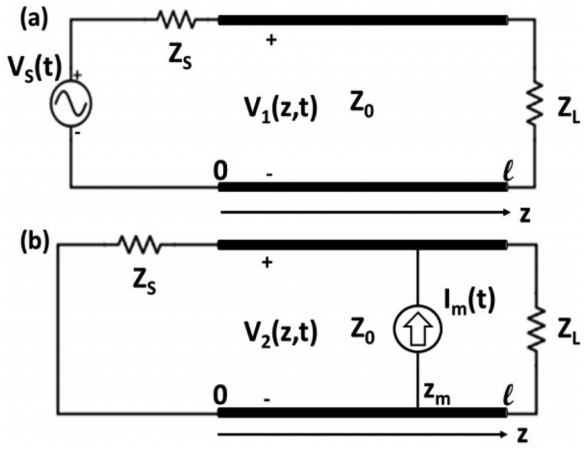

FIG. 7. (a) Transmission line circuit without the multipactor current source but with the voltage source. (b) Transmission line circuit without the voltage source but with the multipactor current source.

A. Calculation of $V_1(z, t)$

For a general complex voltage source $V_S(t)$, as shown in Fig. 7(a), we may first consider the impulse response by assuming $V_S(t) = \delta(t)$, where $\delta(t)$ is the Dirac delta function. The Green's function thus obtained consists of a single impulse that propagates back and forth along the TL between $z = 0$ and $z = l$. At time $t = 0^+$, the voltage pulse (at $z = 0^+$) does not see the load impedance Z_L (since it takes a time $t = l/v$ to reach the load where $v = c$, the light speed on the lossless TL). Thus, the voltage source initially sees the circuit shown in Fig. 8, and the voltage divider relation gives the voltage, $V(z = 0^+, t) = \frac{Z_0}{Z_0+Z_S}\delta(t)$, $t \in (0, \frac{l}{v})$. This voltage pulse travels down the TL undisturbed and thus has the form

$$V(z,t) = \frac{Z_0}{Z_0 + Z_S}\delta\left(t - \frac{z}{v}\right), \quad z \in (0, l), t \in \left(0, \frac{l}{v}\right). \tag{A1}$$

Note that for $t > 0$, the voltage source has a zero value, i.e., it becomes a short circuit, as the voltage source is a delta function (for the Green's function that we are now considering). So for $t > 0$, the TL in Fig. 7(a) is modeled in Fig. 9, on which a forward propagating voltage pulse has been launched. After a transit time (l/v), this initial voltage impulse reaches the load and is reflected, with the

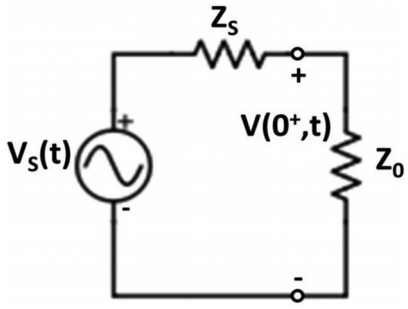

FIG. 8. Voltage divider circuit that the voltage pulse initially sees.

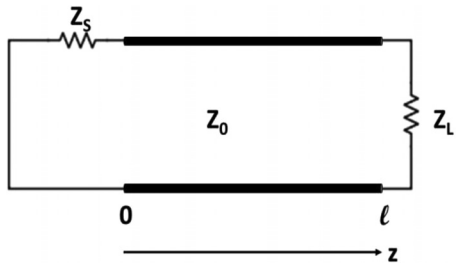

FIG. 9. Transmission line model that a delta-function voltage pulse sees for $t>0$ [Fig. 7(a)]. It is also applicable if the transmission line is excited by a delta-function current pulse [Fig. 7(b)].

reflection coefficient R_L given by Eq. (5b) of the main text. This reflected voltage pulse is then described by

$$V(z,t)=\frac{Z_0}{Z_0+Z_S}R_L\delta\left(t-\frac{2l}{v}+\frac{z}{v}\right),\quad z\in(0,l),t\in\left(\frac{l}{v},\frac{2l}{v}\right). \tag{A2}$$

As this reflected pulse reaches the left end of the TL, $z=0$, it will be further reflected with reflection coefficient, R_S, at the source given by Eq. (5a) of the main text. This reflected voltage pulse traveling to the right is thus

$$V(z,t)=\frac{Z_0}{Z_0+Z_S}R_LR_S\delta\left(t-\frac{2l}{v}-\frac{z}{v}\right),\quad z\in(0,l),t\in\left(\frac{2l}{v},\frac{3l}{v}\right). \tag{A3}$$

This "bouncing back and forth" between the source and load due to impedance mismatches will continue indefinitely. See Fig. 9.

Combining Eqs. (A1)–(A3), and the subsequent pulses, the Green's function for $V_1(z,t)$ becomes

$$\begin{aligned}G(z,t)=\frac{Z_0}{Z_0+Z_S}\Bigg\{&\delta\left(t-\frac{z}{v}\right)+R_L\delta\left(t-\frac{2l}{v}+\frac{z}{v}\right)\\&+\sum_{n=1}^{\infty}(R_LR_S)^n\delta\left(t-\left(\frac{2nl}{v}+\frac{z}{v}\right)\right)\\&+\sum_{n=1}^{\infty}R_L(R_LR_S)^n\delta\left(t-\left(\frac{2(n+1)l}{v}-\frac{z}{v}\right)\right)\Bigg\}.\end{aligned} \tag{A4}$$

For the general voltage source $V_S(t)$ [Fig. 7(a)], we may immediately write down the closed form solution for the voltage $V_1(z,t)$ on the TL, using the Green's function (A4),

$$\begin{aligned}V_1(z,t)=\frac{Z_0}{Z_0+Z_S}\Bigg\{&V_s\left(t-\frac{z}{v}\right)+R_LV_s\left(t-\frac{2l}{v}+\frac{z}{v}\right)\\&+\sum_{n=1}^{\infty}(R_LR_S)^nV_s\left(t-\left(\frac{2nl}{v}+\frac{z}{v}\right)\right)\\&+\sum_{n=1}^{\infty}R_L(R_LR_S)^nV_s\left(t-\left(\frac{2(n+1)l}{v}-\frac{z}{v}\right)\right)\Bigg\},\end{aligned} \tag{A5}$$

which is Eq. (2) of the main text. In the curly bracket of Eq. (A5), the first term represents the first forward traveling wave, the second term represents the first reflected wave from the load, the first infinite sum represents all subsequent rightward propagating waves that are reflected by the mismatches at the source, and the last infinite sum represents all subsequent leftward propagating waves that are reflected by the mismatches at the load.

B. Calculation of $V_2(z, t)$

For a general current source $I_m(t)$, as shown in Fig. 7(b), we may again first consider the impulse response by assuming $I_m(t)=\delta(t)$, where $\delta(t)$ is the Dirac delta function. The Green's function for $V_2(z, t)$ thus obtained consists of two impulses that propagate back and forth on the TL between $z=0$ and $z=l$. At time $t=0^+$, the current pulse (at $z=z_m$) does not see the load impedance Z_L nor the source impedance Z_S. It only sees a TL of impedance Z_0 to its right, and another TL of the same impedance to its left (a current divider). Thus, this current pulse splits into two equal parts at $t=0^+$, one part traveling to the left of $z=z_m$, and an equal part traveling to the right of $z=z_m$.

Note that for $t>0$, the current source has a zero value, i.e., it becomes an open circuit at $z=z_m$, as the current source is a delta function (for the Green's function that we are now considering). So for $t>0$, the TL in Fig. 7(b) is again modeled in Fig. 9, on which two voltage impulses of equal amplitude propagate in opposite directions, from $z=z_m$. We have already solved for the back and forth propagation of an impulse voltage on the TL shown in Fig. 9. The two impulse voltages propagating in opposite directions (initially) just require some book keeping. Analogous to Eq. (A5), we then obtain the closed form solution for the voltage $V_2(z, t)$ on the TL for a general current source $I_m(t)$ [Fig. 7(b)],

$$\begin{aligned}V_2(z,t)=&\frac{Z_0}{2}\Bigg\{I_m\left(t+\frac{z_m}{v}-\frac{z}{v}\right)+R_LI_m\left(t+\frac{z_m}{v}-\frac{2l}{v}+\frac{z}{v}\right)\\&+\sum_{n=1}^{\infty}(R_LR_S)^n\Bigg[I_m\left(t+\frac{z_m}{v}-\left(\frac{2nl}{v}+\frac{z}{v}\right)\right)\\&+R_LI_m\left(t+\frac{z_m}{v}-\frac{2(n+1)l}{v}+\frac{z}{v}\right)\Bigg]\Bigg\}\\&+\frac{Z_0}{2}\Bigg\{I_m\left(t-\left(\frac{z_m}{v}-\frac{z}{v}\right)\right)+R_SI_m\left(t-\left(\frac{z_m}{v}-\frac{2l}{v}+\frac{z}{v}\right)\right)\\&+\sum_{n=1}^{\infty}(R_LR_S)^n\Bigg[I_m\left(t-\frac{z_m}{v}+\left(\frac{2nl}{v}+\frac{z}{v}\right)\right)\\&+R_SI_m\left(t-\frac{z_m}{v}+\frac{2(n+1)l}{v}-\frac{z}{v}\right)\Bigg]\Bigg\},\end{aligned} \tag{A6}$$

which is Eq. (3) of the main text. The aforementioned Green's function for $V_2(z, t)$ is given by Eq. (A6) with $I_m(t)$ being replaced by $\delta(t)$. In Eq. (A6), the first curly bracket represents the current pulse that initially propagates to the right of $z=z_m$, and the second curly bracket represents the current pulse that initially propagates to the left of $z=z_m$.

APPENDIX B: DEFINITION OF THE "I" AND "Q" COMPONENTS

In this Appendix, we define the normalized error vector in terms of the in-phase (I) and quadrature (Q) components that are

displayed in Figs. 2–6. For the single frequency case of Figs. 2–4, the unperturbed (pristine) signal is $V_1(z = l,\ t)$, denoted as

$$f(t) = A\cos(\omega t + \varphi), \tag{B1}$$

with amplitude A, frequency ω, and phase φ. The perturbation to this signal due to multipactor is $V_2(z = l,\ t)$, denoted as $\Delta f(t)$. The I and Q components of the normalized error vector for this single frequency case are defined to be

$$I(t) \equiv \frac{\int_t^{t+T} \Delta f(t') \cdot f(t') dt'}{\int_t^{t+T} f^2(t') dt'} = \frac{\int_t^{t+T} \Delta f(t') \cdot A\cos(\omega t' + \varphi) dt'}{\int_t^{t+T} A^2\cos^2(\omega t' + \varphi) dt'}$$

$$= \frac{2}{AT} \int_t^{t+T} \Delta f(t') \cdot \cos(\omega t' + \varphi) dt', \tag{B2a}$$

$$Q(t) \equiv \frac{\int_t^{t+T} \Delta f(t') \cdot A\sin(\omega t' + \varphi) dt'}{\int_t^{t+T} f^2(t') dt'}$$

$$= \frac{2}{AT} \int_t^{t+T} \Delta f(t') \cdot \sin(\omega t' + \varphi) dt', \tag{B2b}$$

where $T = 2\pi/\omega$. When a steady state occurs in the multipactor current, as in Figs. 2 and 4, the I and Q quantities are strongly correlated upon using the above definitions, as shown in Figs. 2(c) and 4(f). We have changed T to $2T$ and $3T$ in Eqs. (B2a) and (B2b) and found that I and Q were unaffected.

When the input signal has multiple tones, as in Figs. 5 and 6, we calculate the in-phase and quadrature components of the signal perturbation, $\Delta f(t) = V_2(z = l,\ t)$, again using Eqs. (B2a) and (B2b), in which $f(t)$ represents each tone individually. Thus, the effect of the perturbation on each tone is computed, which is shown in Figs. 5(d) and 6(f).

REFERENCES

[1] J. R. M. Vaughan, "Multipactor," IEEE Trans. Electron Devices **35**(7), 1172–1180 (1988).
[2] R. A. Kishek, Y. Y. Lau, L. K. Ang, A. Valfells, and R. M. Gilgenbach, "Multipactor discharge on metals and dielectrics: Historical review and recent theories," Phys. Plasmas **5**(5), 2120–2126 (1998).
[3] F. Piro and Y. Brand, "PIM and multipactor considerations for future high-rf power space missions," in the 8th European Conference on Antennas and Propagation, EuCAP (2014).
[4] *Special Sessions on Multipactor, I and II, IEEE ICOPS* (IEEE, Denver, CO, 2018).
[5] E. Sorolla, S. Anza, B. Gimeno, A. M. Pérez, C. Vicente, J. Gil, F. J. Pérez-Soler, F. D. Quesada, A. Álvarez, and V. E. Boria, "An analytical model to evaluate the radiated power spectrum of a multipactor discharge in a parallel-plate region," IEEE Trans. Electron Devices **55**(8), 2252–2258 (2008).
[6] X. Wang, J. Shen, J. Wang, Q. Song, Z. Wang, Y. Li, R. Wang, T. Hu, Y. Xia, Q. Sun, X. Yin, W. Cui, H. Zhang, X. Zhang, C. Liu, C. Li, and L. Ran, "Monte Carlo analysis of occurrence thresholds of multicarrier multipactors," IEEE Trans. Microwave Theory Tech. **65**(8), 2734–2748 (2017).
[7] M. Jiménez, B. Gimeno, C. Miquel-Espanya, D. Raboso, S. Anza, C. Vicente, J. Gil, F. Quesada, A. Álvarez, M. Taroncher, M. Reglero, and V. E. Boria, "Analysis of the electromagnetic radiation generated by a multipactor discharge occurring within a microwave passive component," J. Phys. D **43**, 395501 (2010).
[8] V. E. Semenov, E. I. Rakova, N. A. Zharova, J. Rasch, D. Anderson, and J. Puech, "Simple model of the rf noise generated by multipacting electrons," J. Phys. D **47**, 055206 (2014).
[9] S. K. Nagesh, D. Revannasiddiah, and S. V. K. Shastry, "Investigation of multipactor breakdown in communication satellite microwave co-axial systems," Pramana **64**(1), 95–110 (2005).
[10] T. P. Graves, "Experimental investigation of electron multipactor discharges at very high frequencies," Ph.D. dissertation (MIT, 2006).
[11] R. Kishek and Y. Y. Lau, "Interaction of multipactor discharge and rf circuit," Phys. Rev. Lett. **75**(6), 1218–1221 (1995).
[12] L. K. Ang, Y. Y. Lau, R. A. Kishek, and R. M. Gilgenbach, "Power deposited on a dielectric by multipactor," IEEE Trans. Plasma Sci. **26**(3), 290–295 (1998).
[13] L. Zhang, Y. Li, S. Lin, H. Wang, C. Liu, J. Li, and Z. Xu, "Numerical simulation and analysis of passive intermodulation caused by multipaction," Phys. Plasmas **25**, 082301 (2018).
[14] J. R. Wilkerson, K. G. Gard, A. G. Schuchinsky, and M. B. Steer, "Electro-thermal theory of intermodulation distortion in lossy microwave components," IEEE Trans. Microwave Theory Tech. **56**(12), 2717–2725 (2008).
[15] M. Tencer, Microelectron. Reliab. **48**, 584 (2008).
[16] D. Seron, C. Collado, J. Mateu, and J. M. O'Callaghan, "Analysis and simulation of distributed nonlinearities in ferroelectrics and superconductors for microwave applications," IEEE Trans. Microwave Theory Tech. **54**(3), 1154–1160 (2006).
[17] D. González-Iglesias, O. Monerris, B. G. Martínez, M. E. Díaz, V. E. Boria, and P. M. Iglesias, "Multipactor RF breakdown in coaxial transmission lines with digitally modulated signals," IEEE Trans. Electron Devices **63**(10), 4096–4103 (2016).
[18] ECSS, "Space engineering: Multipaction design and test," Report No. ECSS-E-20-01A Rev. 1 (2013).
[19] V. Semenov, M. Buyanova, D. Anderson, M. Lisak, R. Udiljak, and J. Puech, "Multipactor in microwave transmission systems using quadrature phase-shift keying," IEEE Trans. Plasma Sci. **38**(4), 915–922 (2010).
[20] D. González-Iglesias, M. P. B. Rodríguez, O. M. Belda, B. Gimeno, V. E. Boria, D. Raboso, and V. E. Semenov, "Analysis of multipactor effect using a phase-shift keying single-carrier digital modulated signal," IEEE Trans. Electron Devices **60**(8), 2664–2670 (2013).
[21] M. Siddiqi and R. Kishek, "A predictive model for multipactor discharge in coaxial systems based on chaos theory," IEEE Trans. Electron Devices **66**(10), 4403–4407 (2019).
[22] E. Sorolla and M. Mattes, "Multipactor saturation in parallel-plate waveguides," Phys. Plasmas **19**, 072304 (2012).
[23] R. Udiljak, D. Anderson, M. Lisak, V. E. Semenov, and J. Puech, "Multipactor in a coaxial transmission line. I. Analytical study," Phys. Plasmas **14**, 033508 (2007).
[24] E. Sorolla, A. Sounas, and M. Mattes, "Space charge effects for multipactor in coaxial lines," Phys. Plasmas **22**, 033512 (2015).
[25] A. M. Pérez, C. Tienda, C. Vicente, S. Anza, J. Gil, B. Gimeno, V. E. Boria, and D. Raboso, "Prediction of multipactor breakdown thresholds in coaxial transmission lines for traveling, standing, and mixed waves," IEEE Trans. Plasma Sci. **37**(10), 2031–2040 (2009).
[26] S. Lin, H. Wang, Y. Li, C. Liu, N. Zhang, W. Cui, and A. Neuber, "Multipactor threshold calculation of coaxial transmission lines in microwave applications with nonstationary statistical theory," Phys. Plasmas **22**, 082114 (2015).
[27] I. A. Kossyi, G. S. Luk'yanchikov, V. E. Semenov, N. A. Zharova, D. Anderson, M. Lisak, and J. Puech, "Experimental and numerical investigation of multipactor discharges in a coaxial waveguide," J. Phys. D **43**, 345206 (2010).
[28] P. Y. Wong, Y. Y. Lau, P. Zhang, N. Jordan, R. M. Gilgenbach, and J. Verboncoeur, "The effects of multipactor on the quality of a signal," in IEEE International Vacuum Electronics Conference (IVEC), April, Pusan, South Korea (2019).

[29]R. A. Kishek, "Ping-pong modes and higher-periodicity multipactor," Phys. Plasmas **20**, 056702 (2013).
[30]C. J. Lingwood, G. Burt, A. C. Dexter, J. D. A. Smith, P. Goudket, and P. H. Stoltz, "Phase space analysis of multipactor saturation in rectangular waveguide," Phys. Plasmas **19**, 032106 (2012).
[31]D. González-Iglesias, A. M. Pérez, S. Anza, J. Vague, B. Gimeno, V. E. Boria, D. Raboso, C. Vicente, J. Gil, F. Caspers, and L. Conde, "Multipactor in a coaxial line under the presence of an axial DC magnetic field," IEEE Electron Dev. Lett. **33**(5), 727–729 (2012).
[32]S. Ramo, "Currents induced by electron motion," Proc. IRE **27**(9), 584–585 (1939); W. Shockley, "Currents to conductors induced by a moving point charge," J. Appl. Phys. **9**, 635 (1937).
[33]J. R. M. Vaughan, "A new formula for secondary emission yield," IEEE Trans. Electron Devices **36**(9), 1963–1967 (1989).
[34]C. Vicente, M. Mattes, D. Wolk, H. L. Hartnagel, J. R. Mosig, and D. Raboso, "Contribution to the RF breakdown in microwave devices and its prediction," in *Proceedings of the 2006 Power Modulator Symposium* (IEEE, New York, 2006), pp. 22–27.
[35]A. Iqbal, J. Verboncoeur, and P. Zhang, "Temporal multiparticle Monte Carlo simulation of dual frequency single surface multipactor," Phys. Plasmas **26**, 024503 (2019).
[36]P. Zhang, Y. Y. Lau, M. Franzi, and R. M. Gilgenbach, "Multipactor susceptibility on a dielectric with a biased dc electric field and a background gas," Phys. Plasmas **18**, 053508 (2011).
[37]C. Chang, C. Z. Liu, C. X. Tang, and L. X. Yan, "The influence of space charge shielding on dielectric multipactor," Phys. Plasmas **16**, 053506 (2009).
[38]V. Semenov, A. Kryazhev, D. Anderson, and M. Lisak, "Multipactor suppression in amplitude modulated radio frequency fields," Phys. Plasmas **8**(11), 5034 (2001).